



# Direct observations of organic aerosols in common wintertime hazes in North China: insights into direct emissions from Chinese residential stoves

Shurui Chen<sup>1</sup>, Liang Xu<sup>1</sup>, Yinxiao Zhang<sup>1</sup>, Bing Chen<sup>1</sup>, Xinfeng Wang<sup>1</sup>, Xiaoye Zhang<sup>2</sup>, Mei Zheng<sup>3</sup>, Jianmin Chen<sup>1,4</sup>, Wenxing Wang<sup>1</sup>, Yele Sun<sup>5</sup>, Pingqing Fu<sup>5</sup>, Zifa Wang<sup>5</sup>, and Weijun Li<sup>1</sup>

<sup>1</sup>Environment Research Institute, Shandong University, Jinan, Shandong 250100, China

<sup>2</sup>Key Laboratory of Atmospheric Chemistry, Chinese Academy of Meteorological Sciences, Beijing 100081, China

<sup>3</sup>State Key Joint Laboratory of Environmental Simulation and Pollution Control, College of Environmental Sciences and Engineering, Peking University, Beijing 100871, China

<sup>4</sup>Shanghai Key Laboratory of Atmospheric Particle Pollution and Prevention, Department of Environmental Science and Engineering, Fudan University, Shanghai 200433, China

<sup>5</sup>State Key Laboratory of Atmospheric Boundary Layer Physics and Atmospheric Chemistry, Institute of Atmospheric Physics, Chinese Academy of Sciences, Beijing 100029, China

Correspondence to: Weijun Li (liweijun@sdu.edu.cn)

Received: 9 June 2016 – Published in Atmos. Chem. Phys. Discuss.: 23 June 2016

Revised: 5 October 2016 – Accepted: 9 January 2017 – Published: 27 January 2017

**Abstract.** Many studies have focused on the physicochemical properties of aerosol particles in unusually severe haze episodes in North China instead of the more frequent and less severe hazes. Consistent with this lack of attention, the morphology and mixing state of organic matter (OM) particles in the frequent light and moderate (L & M) hazes in winter in the North China Plain (NCP) have not been examined, even though OM dominates these fine particles. In the present work, morphology, mixing state, and size of organic aerosols in the L & M hazes were systematically characterized using transmission electron microscopy coupled with energy-dispersive X-ray spectroscopy, atomic force microscopy, and nanoscale secondary ion mass spectrometer, with the comparisons among an urban site (Jinan, S1), a mountain site (Mt. Tai, S2), and a background island site (Changdao, S3) in the same hazes. Based on their morphologies, the OM particles were divided into six different types: spherical (type 1), near-spherical (type 2), irregular (type 3), domelike (type 4), dispersed-OM (type 5), and OM-coating (type 6). In the three sampling sites, types 1–3 of OM particles were most abundant in the L & M hazes and most of them were internally mixed with non-OM particles. The abundant near-spherical OM particles with higher sphericity and lower aspect ratio indicate that these primary OM particles formed in the cool-

ing process after polluted plumes were emitted from coal combustion and biomass burning. Based on the Si-O-C ratio in OM particles, we estimated that 71 % of type 1–3 OM particles were associated with coal combustion. Our result suggests that coal combustion in residential stoves was a widespread source from urban to rural areas in NCP. Average OM thickness which correlates with the age of the air masses in type 6 particles only slightly increased from S1 to S2 to S3, suggesting that the L & M hazes were usually dry (relative humidity < 60 %) with weak photochemistry and heterogeneous reactions between particles and gases. We conclude that the direct emissions from these coal stoves without any pollution controls in rural areas and in urban outskirts contribute large amounts of primary OM particles to the regional L & M hazes in North China.

## 1 Introduction

Atmospheric particulate matter is composed of diverse chemical compounds, both organic and inorganic matters. Organic aerosol particles are of two types: primary organic aerosol (POA), directly emitted from fossil fuel combustion, biomass burning, vehicular exhaust, and cooking; and

secondary organic aerosol (SOA), formed from the oxidation of gaseous volatile organic compounds (Kanakidou et al., 2005). Organic aerosols account for 18–70 % of the non-refractory submicron aerosol particles in the atmosphere (Zhang et al., 2007). It is well known that organic aerosols affect the atmosphere through the interaction with reactive trace gases, water vapor, clouds, precipitation, and radiation (Fuzzi et al., 2006). Organic aerosols also influence the physical and chemical properties (e.g., size, light absorptivity, and hygroscopicity) of other particles; they directly affect visibility and climate by scattering and absorbing solar radiation (Pöschl, 2005; Kanakidou et al., 2005; Kulmala et al., 2004). Although most organic aerosol components are known to have a cooling effect on global climate, brown carbon in organic aerosols can absorb solar radiation at shorter wavelengths and lead to warming (Alexander et al., 2008). Moreover, many organic compounds (e.g., benzene, polycyclic aromatic hydrocarbons (PAHs), toluene) which are toxic to humans and other biological species have been found in atmospheric particles (Mauderly and Chow, 2008).

In recent years, haze episodes have become one of the most serious environmental problems in China, following the rapid urbanization and population growth in eastern China. The Ministry of Environmental Protection of the People's Republic of China, on 1 January 2013, started to monitor daily  $\text{PM}_{2.5}$  (aerodynamic equivalent diameter of particles  $\leq 2.5 \mu\text{m}$ ) concentrations and defined the daily average air quality levels as excellent ( $0\text{--}35 \mu\text{g m}^{-3}$ ), good ( $35\text{--}75 \mu\text{g m}^{-3}$ ), light ( $75\text{--}115 \mu\text{g m}^{-3}$ ), moderate ( $115\text{--}150 \mu\text{g m}^{-3}$ ), heavy ( $150\text{--}250 \mu\text{g m}^{-3}$ ), and severe ( $> 250 \mu\text{g m}^{-3}$ ) (Chinese National Ambient Air Quality Standards). Haze as a weather phenomenon is defined by visibility  $\leq 10 \text{ km}$  and relative humidity (RH)  $\leq 80 \%$  (Chinese Meteorological Industry Standard). Previous studies have shown that haze levels normally are associated with different levels of  $\text{PM}_{2.5}$  concentrations and RH (Shen et al., 2015; Wang et al., 2006; Chen et al., 2014). Based on their results, we classify severe haze days ( $< 5 \text{ km}$ ) with  $\text{PM}_{2.5}$  concentrations  $\geq 250 \mu\text{g m}^{-3}$  and light ( $8\text{--}10 \text{ km}$ ) to moderate ( $5\text{--}8 \text{ km}$ ) haze days at  $75\text{--}250 \mu\text{g m}^{-3}$ , both with RH  $< 80 \%$ .

Because of their unusually high  $\text{PM}_{2.5}$  concentrations ( $> 250 \mu\text{g m}^{-3}$ ) and low visibility ( $< 5 \text{ km}$ ), the physicochemical properties of aerosol particles in severe wintertime hazes in China are well understood (Huang et al., 2014; Guo et al., 2014; Zheng et al., 2015). Recently, Zheng et al. (2015) suggested that characteristics of aerosol particles in severe hazes would not be the same in L & M hazes. Although this knowledge is critical to understand severe haze formation and its impacts on human health, the frequency of severe haze episodes is low and their duration is short. For example, we statistically analyzed haze days during the winter ( $\sim 92$  days) of 2014–2015 in nine cities. Figure S1 in the Supplement shows that light and moderate (L & M) haze days occurred 22–63 % of the time and that severe haze days were less frequent at 4–32 %, with the variation dependent on location

within the NCP. The city of Jinan was an example showing the timescale of severe and L & M haze episodes (Fig. S2). Compared to severe hazes, the L & M hazes were most frequent in winter and lasted longer in the NCP. Therefore, understanding aerosol particles in the more common L & M hazes in the NCP is important to further evaluate their impacts on human health and regional climate.

Various “bulk” analytical instruments have been used to study organic aerosol particles during haze episodes. High-resolution time-of-flight aerosol mass spectrometry (HR-AMS) was applied to determine the mass concentrations and bulk composition of organic aerosols (Sun et al., 2010). Gas chromatography–mass spectrometry (GC-MS) provided chemical composition and structures of organics in aerosols (Fu et al., 2012; Wang et al., 2009). It should be noted that bulk analytical techniques only provide average properties of  $\text{PM}_{2.5}$  and the mixing state, phase, and morphology of organic particles remain unknown. Detailed information about individual organic particles, moreover, is critical to evaluate their formation, sources, and their hygroscopic and optical properties in the atmosphere. For example, considerable numbers of tar balls containing homogeneous brown carbon (BrC) occur in the smoldering smoke from biofuels (Chakrabarty et al., 2010, 2013; Adachi and Buseck, 2011; Alexander et al., 2008; China et al., 2013; Hand et al., 2005; Posfai et al., 2004). Atmospheric particles undergo liquid–liquid phase separations and go on to form OM coatings on inorganic aerosol particles (You et al., 2012). The surface coating by OM on individual particles influences water uptake and evaporation of individual particles and their heterogeneous reactions in the atmosphere (Shiraiwa et al., 2011; Zawadowicz et al., 2015; Riipinen et al., 2011). Despite the importance of these phenomena, the morphology and mixing state of OM particles in wintertime L & M hazes in the NCP have not been examined, although OM is dominant in fine particles (Sun et al., 2013).

To characterize organic aerosols in greater detail in L & M hazes, individual particles in the NCP in winter were analyzed using different individual particle instruments. Morphology, mixing state, and size of organic aerosols were systematically characterized and compared at the three sampling sites (background island site, mountain site, and urban site) in the same haze. This information enables the discussion of source and ageing mechanisms of OM particles, which leads to insights about the formation of regional wintertime L & M hazes in the NCP.

## 2 Experimental methods

### 2.1 Sampling sites and particle collection

$\text{PM}_{2.5}$  and individual particle samples were simultaneously collected during 13–23 December 2014 at three sampling sites: an urban site (S1), a mountain site (S2), and a background site (S3) in the NCP (Fig. 1).



**Figure 1.** Regional haze layer covering the North China Plain: S1 (urban Jinan), S2 (top of Mt. Tai), and S3 (Changdao Island) sites. The MODIS images on 14 and 19 December show a grey haze layer during the light and moderate regional hazes over the NCP.

S1, an urban site in Jinan (53.9 m a.s.l.; 36.67° N, 116.98° E), is 50 km north of S2. S1 is a typical polluted city with high-density residential areas surrounded by large industrial zones (W. J. Li et al., 2011b). Inhabitants in Jinan use coal for central heating in wintertime. People living in the outskirts of Jinan (50 km away from Jinan urban center) use stoves to burn coal for cooking and heating in winter. Aerosol particles collected at S1 were mainly fresh particles and can reflect the emissions from local urban and industrial, residential stoves in winter.

S2, at the top of Mt. Tai (1534 m a.s.l.; 36.251° N, 117.101° E), is the highest mountain in the middle of the NCP, ~230 km inland from the Bohai and Yellow seas. S2 is the perfect location to observe air pollutants near the planetary atmospheric layer over the NCP. Aerosol particles collected at S2 were aged particles and represent regional transport in the NCP (W. Li et al., 2011).

S3, Changdao Island, the National Station for Background Atmospheric Monitoring site (153 m a.s.l.; 38.19° N, 120.74° E), is in the Bohai Sea. During the winter monsoon season, S3 is downwind of the Jing-Jin-Ji area (i.e., cities of Beijing and Tianjin and Hebei province) and Shandong province (Feng et al., 2012). Therefore, S3 serves as a polluted background site due to the transport of continental air. Therefore, aerosol particles collected at the three sampling sites represent the different pollutant characteristics of polluted urban air, upper air layer, and background island air in the NCP.

PM<sub>2.5</sub> was collected on 90 mm quartz filters for 11.5 h (daytime: 07:30–19:00; nighttime: 19:30–07:00 (next day)) using three KB-120 samplers at a flow rate of 100 L min<sup>-1</sup>. The quartz filters were stored in a refrigerator for OC, EC, and water-soluble ion analysis. In the study, OC and EC concentrations of 70 quartz filters were analyzed by an OC / EC analyzer (Sunset Lab) and water-soluble ions (i.e., K<sup>+</sup>, Na<sup>+</sup>, Ca<sup>2+</sup>, Mg<sup>2+</sup>, NH<sub>4</sub><sup>+</sup>, SO<sub>4</sub><sup>2-</sup>, NO<sub>3</sub><sup>-</sup>, and Cl<sup>-</sup>) by an ion chromatography system (Dionex ICs-90). Three single-stage cascade impactors with a 0.5 mm diameter jet nozzle at a flow

rate of 1.0 L min<sup>-1</sup> were used to collect particles onto copper transmission electron microscope (TEM) grids coated with carbon film (carbon type-B, 300-mesh copper, Tianld Co., China). Individual particle samples were collected at the same time everyday at three sites. The sampling duration were different based on the different levels of air quality (Table S2 in the Supplement). The collection efficiency of the impactor is 50 % for particles with an aerodynamic diameter of 0.25 μm and with a density of 2 g cm<sup>-3</sup> (W. Li et al., 2011). After sample collection, the Cu grids were placed in a sealed, dry and clean environment until the TEM analysis. Based on their distribution of samples, 11 aerosol samples (Table S2) at each sampling site were selected and analyzed by the TEM.

## 2.2 TEM analyses

The JEOL JEM-2100 transmission electron microscopy operated at 200 kV with energy-dispersive X-ray spectrometry (TEM/EDX) was used to analyze individual particles. An energy-dispersive X-ray spectrometer (EDX) can detect elements heavier than carbon. EDX spectra were acquired for 15 s to minimize the potential beam damage. TEM grids are made of copper (Cu), so Cu is excluded in the analyses. The distribution of particles on the TEM grids was not uniform: coarser particles were deposited near the center and finer particles dispersed on the fringe. To make sure that the analyzed particles were representative of the entire size range, three to four areas were chosen from the center and periphery of the sampling spot on each sample.

## 2.3 NanoSIMS analysis

After the TEM analysis, three typical samples were chosen for nanoscale secondary ion mass spectrometer analysis (NanoSIMS 50L, CAMECA Instruments, Geneviers, France), an ultrahigh vacuum technique for surface and thin-film analysis at the Institute of Geology and Geophysics, Chinese Academy of Sciences. In this study, <sup>12</sup>C<sup>-</sup>, <sup>16</sup>O<sup>-</sup>,

$^{12}\text{C}^{14}\text{N}^-$ ,  $^{14}\text{N}^{16}\text{O}_2^-$ , and  $^{32}\text{S}^-$  ions in individual particles were obtained when the  $\text{Cs}^+$  primary ion beam caused the ionization of atoms within the particles. Furthermore, ion intensity mappings of individual particles with nanometer resolution can show the distribution of different ions.  $^{12}\text{C}^-$  and  $^{12}\text{C}^{14}\text{N}^-$  represent the organic matter in individual particles (Chi et al., 2015; Ghosal et al., 2014; K. Li et al., 2016).

## 2.4 AFM analysis

Atomic force microscopy (AFM) with a tapping mode analyzed aerosol particles under ambient conditions. AFM, using a digital Nanoscope IIIa instrument, can determine the three-dimensional morphology of particles. The AFM settings contain imaging forces between 1 and 1.5 nN, scanning rates between 0.5 and 0.8 Hz, and scanning range sizes at  $10\ \mu\text{m}$  with a resolution of 512 pixels per length. After the AFM analysis, composition of the same particles was confirmed by TEM, with 20 (S1), 25 (S2), and 13 (S3) individual particles analyzed by this method for each of the three sampling sites. The Nanoscope analysis software can automatically obtain bearing area ( $A$ ) and bearing volume ( $V$ ) of each analyzed particle according to the formulas described by Chi et al. (2015).

The definition and relationship of equivalent circle diameter (ECD,  $x$ ) and equivalent volume diameter (EVD,  $y$ ) are shown in Fig. S3 in the Supplement ( $\text{EVD} = 0.8334 \text{ECD}$  (S1),  $\text{EVD} = 0.7286 \text{ECD}$  (S2), and  $\text{EVD} = 0.6601 \text{ECD}$  (S3)). Therefore, the ECD ( $x$ ) of individual aerosol particles measured from the iTEM software can be further converted into EVD ( $y$ ) based on these relationships.

## 3 Results

### 3.1 Regional haze periods in the North China Plain

Aerosol particles were collected in three regional L & M hazes during 13–23 December 2014 (Fig. S4). Moderate Resolution Imaging Spectroradiometer (MODIS) images on 14 and 19 December 2014 clearly display a regional haze layer covering the three sampling sites in the NCP (Fig. 1). The average  $\text{PM}_{2.5}$  concentrations were  $96.6\ \mu\text{g m}^{-3}$  (range:  $79\text{--}171\ \mu\text{g m}^{-3}$ ) at S1,  $88.6\ \mu\text{g m}^{-3}$  (range:  $76\text{--}110\ \mu\text{g m}^{-3}$ ) at S2, and  $80.3\ \mu\text{g m}^{-3}$  (range:  $75\text{--}84\ \mu\text{g m}^{-3}$ ) at S3 on haze days, twice as high as on clear days (52, 48, and  $32.3\ \mu\text{g m}^{-3}$ ) during the sampling period. The RH at all three sampling sites was lower than 60 % during the sampling period (Fig. S5).

The average concentrations of OC, EC, OC/EC, water-soluble ions and their mass proportions in  $\text{PM}_{2.5}$  were much higher on haze days than on clear days at three sampling sites (Table S1). OC on haze days was more than 1.7 times higher than that on clear days at three sites. We found that the fraction of OC to  $\text{PM}_{2.5}$  remained fairly stable regardless of L & M haze and clear days. OM concentration was esti-

ated at  $20\text{--}33\ \mu\text{g m}^{-3}$  and OM/ $\text{PM}_{2.5}$  ratio was at the range of 23–34 % during haze days in the NCP (Table S1).

### 3.2 Morphology of organic particles

Based on morphology and chemical composition of individual particles using TEM/EDX, we identified five types of particles: sulfates (including K-rich sulfate and ammonium sulfate), fly ash/metal, mineral, soot, and OM-like particles (Figs. 2 and S6). These results are consistent with previous studies during the haze episodes in the NCP (Li et al., 2012; W. J. Li et al., 2011b). In order to remove the interference of the carbon substrate on TEM grids, a nanoSIMS was employed to verify OM-like particles through  $^{12}\text{C}^{14}\text{N}^-$  and  $^{12}\text{C}^-$  mappings (Figs. 3 and S7). Figure 3 clearly shows that one near-spherical particle, which contains C, O, and minor Si on TEM grids, displays strong  $\text{CN}^-$  and  $\text{O}^-$  signals but no clear  $\text{NO}_2^-$  and  $\text{S}^-$  signals. As a result, this type of particle can be confirmed as the OM particle (K. Li et al., 2016; Ghosal et al., 2014). TEM analysis showed that OM-containing particles were most abundant in all the haze samples, accounting for 70 % of the 5090 analyzed particles (Fig. 2).

Based on the morphology of OM particles, they were divided into six different types: spherical (type 1, Fig. 4a), near-spherical (type 2, Fig. 4b), irregular (type 3, Fig. 4c), domelike (type 4, Fig. 4d), dispersed-OM (type 5, Fig. 4e), and OM-coating (type 6, Fig. 4f). Here, the domelike particles look like transparent droplet-like particles in TEM images.

Because the high-resolution TEM images of individual particles can clearly display particle interior mixing structures, it allows us to identify OM particles based on their different shapes in OM-containing particles (Fig. S6). Figure 2 shows that the proportions of types 1–3 in OM particles was 73 %, following type 4 at 5 %, type 5 at 13 %, and type 6 at 14 % for the three sites as a whole. Further, we measured the projected area, the perimeter, the maximum projected length, and the maximum projected width of 967 selected OM particles. From these data, the sphericity (Sph) and aspect ratio (AR) of different types of OM particles were calculated, which characterize their shape and thereby imply their ageing during transport and their emission sources (W. Li et al., 2016). The Sph and AR were defined by the following formulas referred to by Li et al. (2013).

#### 3.2.1 Sphericity (Sph)

Sphericity describes the sphericity or “roundness” of the measured object by using central moments. A sphericity of 1 (the highest value) indicates a particle is perfectly spherical.

$$\text{Sph} = \frac{\sqrt{4\pi S}}{P} = \frac{\sqrt{4\pi\pi R_1^2}}{2\pi R_2} = \frac{R_1}{R_2}. \quad (1)$$

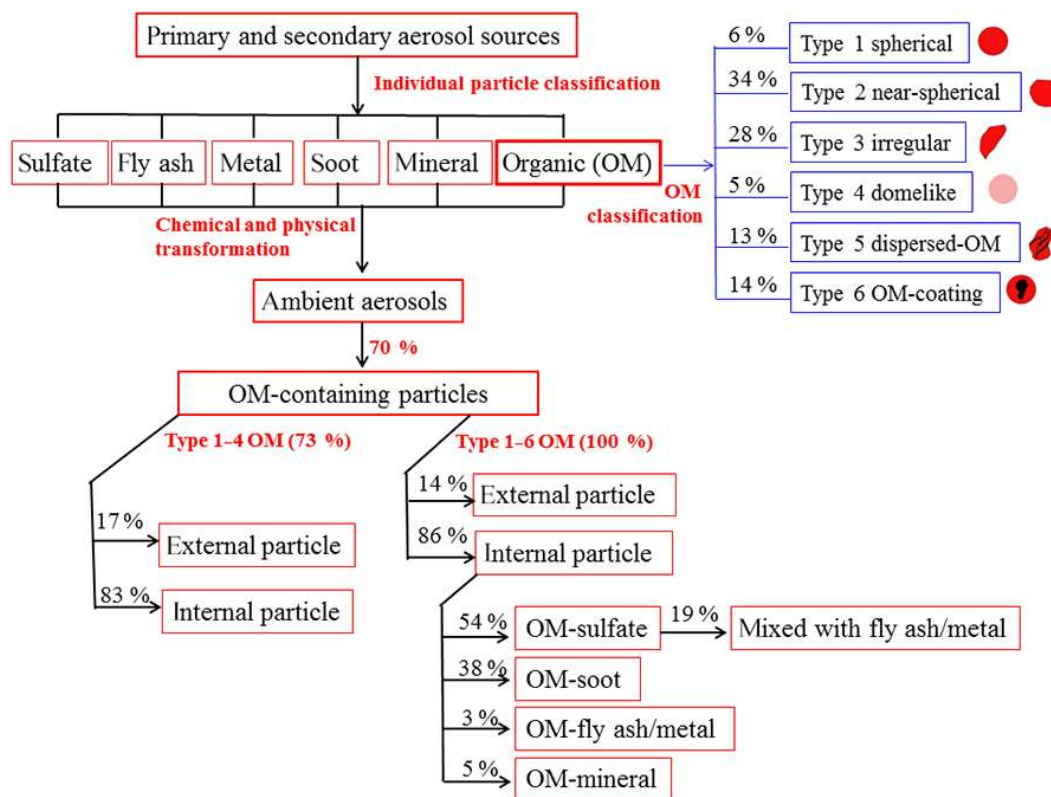


**Figure 2.** Flowchart of individual aerosol particles classification in L & M haze episodes in NCP based on TEM/EDX. A total of 5090 individual particles were analyzed using TEM/EDX.

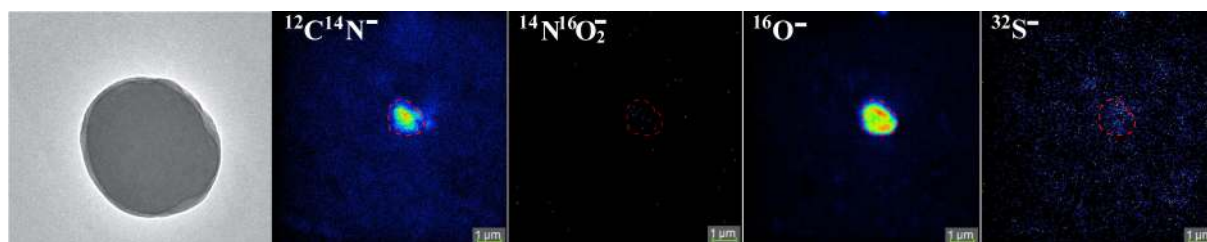


**Figure 3.** NanoSIMS-based ion intensity mappings of  $^{12}\text{C}^{14}\text{N}^-$ ,  $^{14}\text{N}^{16}\text{O}_2^-$ ,  $^{16}\text{O}^-$ , and  $^{32}\text{S}^-$  from a near-spherical OM particle.

### 3.2.2 Aspect ratio (AR)

The maximum ratio of length and width of a bounding rectangle for the measured object is the aspect ratio. An aspect ratio of 1 (the lowest value) indicates a particle is not elongated in any direction.

$$\text{AR} = \frac{L_{\max}}{W_{\max}}, \quad (2)$$

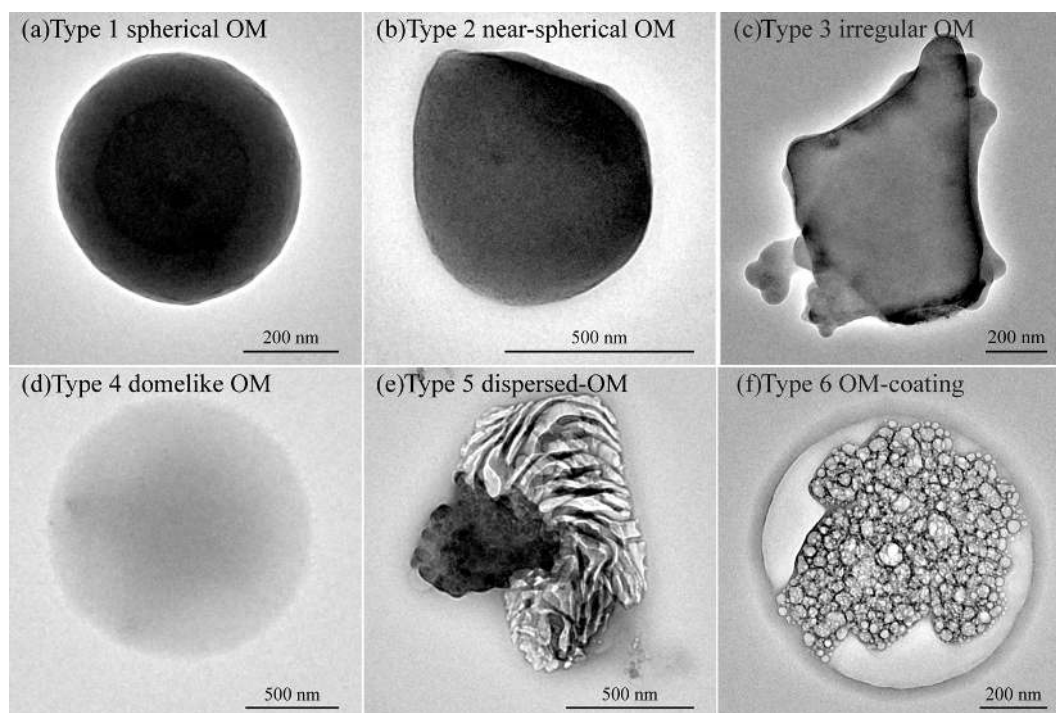
where  $S$  is projected area,  $R_1$  is equivalent area radius,  $P$  is perimeter,  $R_2$  is equivalent perimeter radius,  $L_{\max}$  is the maximum projected length, and  $W_{\max}$  is the maximum projected width.

Table 1 displays the Sph and AR of individual OM particles measured by the iTEM software. At the three different

sampling sites, OM particles were in the fine range with diameters  $< 1 \mu\text{m}$ . The statistics shows that spherical OM particles exhibited the highest Sph at 0.96–0.99 and the lowest AR at 1.01–1.03 at the three sites, followed by OM coating (Sph: 0.88–0.93, AR: 1.06–1.08), near-spherical OM (Sph: 0.82–0.83, AR: 1.12–1.13), domelike OM (Sph: 0.63–0.73, AR: 1.24–1.40), irregular OM (Sph: 0.51–0.57, AR: 1.39–1.48) and dispersed-OM particles (Sph 0.50–0.58, AR: 1.35–1.49).

### 3.3 Mixing state of OM particles

Although we identified different types of OM particles in individual particles, 86 % of OM particles were internally mixed with non-OM particles, such as soot, mineral, fly ash,



**Figure 4.** Typical TEM images of different types of OM particles. (a) Type 1: spherical shape; (b) type 2: near-spherical shape; (c) type 3: irregular shape; (d) type 4: domelike OM (droplet-like particle); (e) type 5: dispersed-OM; (f) type 6: OM-coating.

**Table 1.** Average size, number, sphericity, and aspect ratio for different OM types at the three sampling sites.

Sampling site	Type	Average size (nm)	Number	Average Sph	Average AR
S1	Type 1, spherical	408	18	0.97	1.02
	Type 2, near-spherical	349	79	0.82	1.13
	Type 3, irregular	539	151	0.51	1.48
	Type 4, domelike	759	23	0.64	1.40
	Type 5, dispersed-OM	751	64	0.50	1.49
	Type 6, OM-coating	672	12	0.93	1.06
S2	Type 1, spherical	282	22	0.96	1.03
	Type 2, near-spherical	323	68	0.83	1.12
	Type 3, irregular	399	62	0.57	1.41
	Type 4, domelike	511	25	0.73	1.24
	Type 5, dispersed-OM	847	34	0.58	1.42
	Type 6, OM-coating	776	66	0.88	1.08
S3	Type 1, spherical	392	27	0.99	1.01
	Type 2, near-spherical	373	122	0.83	1.12
	Type 3, irregular	375	117	0.57	1.39
	Type 4, domelike	706	14	0.63	1.35
	Type 5, dispersed-OM	575	35	0.55	1.35
	Type 6, OM-coating	828	28	0.93	1.06

metal, and sulfate particles (Figs. 2 and S6). Based on their morphological mixing state, we discriminated four OM internally mixed particles: OM-soot (Figs. 5a and S8), OM-mineral (Fig. 5b), OM-fly ash/metal (Fig. 5c), and OM-sulfate particles (Fig. 5d–e). Our results show that 83 % of

type 1–4 OM particles were attached to soot, mineral, sulfate, and metal particles; only 17 % of type 1–4 OM particles were externally mixed particles; and all the type 5–6 OM particles were internally mixed with sulfate particles (Fig. 2). In addition, the major OM internally mixed particles include 54 %

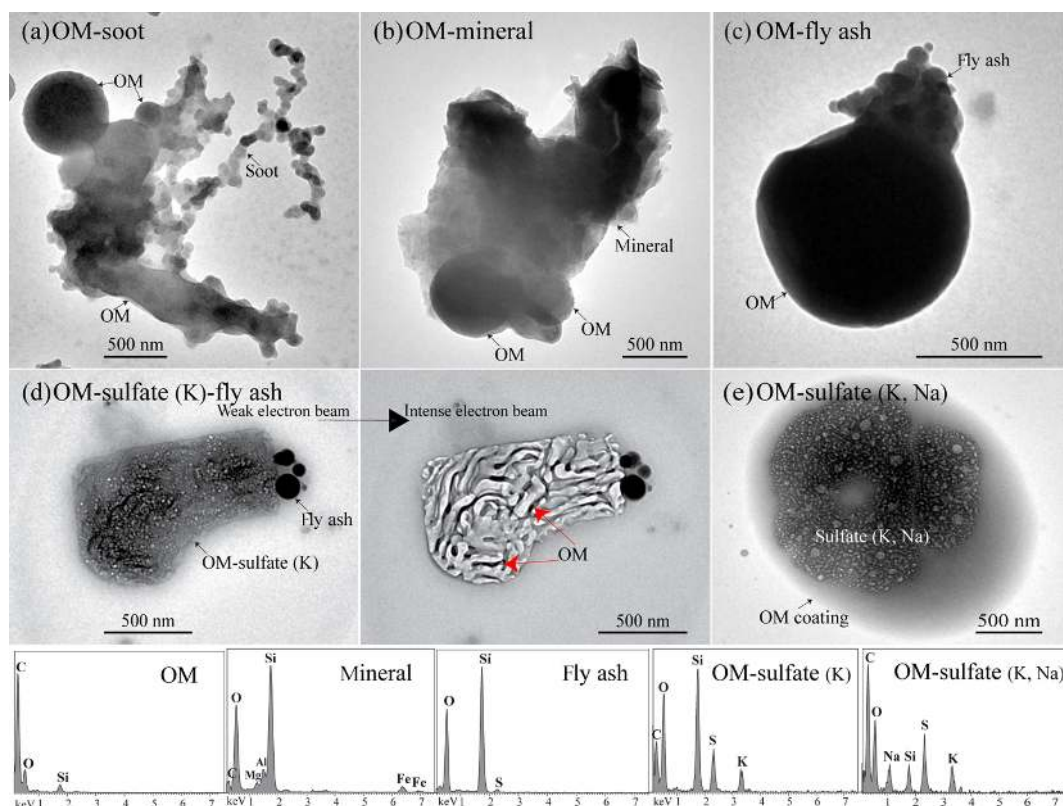


**Figure 5.** Typical TEM images of OM internally mixed particles (a) a spherical OM particle attached to a soot particle, (b) a near-spherical OM particle attached to a mineral particle, (c) fly ash particles attached to a near-spherical OM particle, (d) OM mixed with sulfate (K)-fly ash particle and its sublimed particle under strong electron beam, and (e) OM as a coating mixed with a sulfate (K, Na) particle. The element compositions in OM, mineral, fly ash, and sulfate particles were measured by the TEM/EDX.

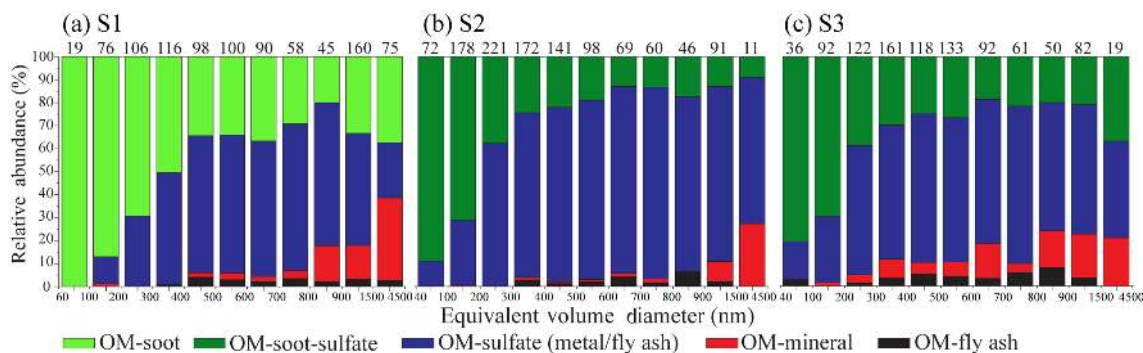


**Figure 6.** Number fractions of OM internally mixed particles at (a) the S1 site (urban Jinan), (b) S2 site (top of Mt. Tai), and (c) S3 site (polluted background). The number of analyzed particles in different size ranges is shown above each column.

OM-sulfate particles and 38% OM-soot particles, followed by 5% OM-mineral particles and 3% OM-fly ash/metal particles (Fig. 2). Based on these analyses, a flowchart of classification of individual aerosol particles is summarized in Fig. 2.

Figure 6 shows number fractions of OM internally mixed particles in different size bins from 0.04 to 4.5  $\mu\text{m}$  at the three sampling sites. OM-soot particles commonly occurred

at S1, but they were mixed with certain amounts of sulfates at S2 and S3 during the sampling period (Fig. S8). OM-soot-containing particles dominated in the finer size range (< 300 nm) at the three sampling sites (Fig. 6). In addition, 19% of OM-sulfate particles were internally mixed with inclusions (i.e., fly ash and metal) at all the three sampling sites (Fig. 2).

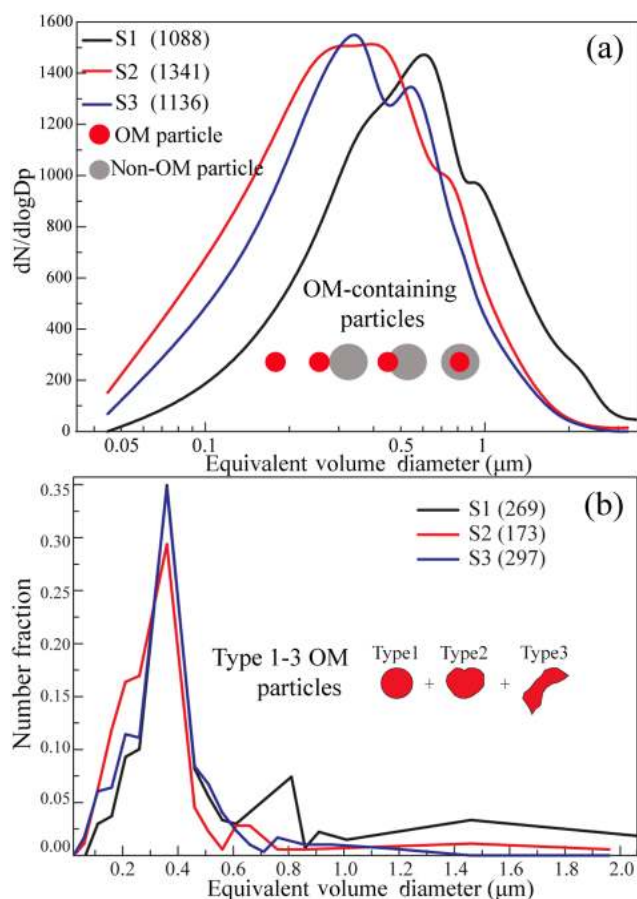


**Figure 7.** Size distributions of OM-containing particles and OM particles during L & M haze episodes. **(a)** Size distributions of 1088, 1341 and 1136 OM-containing particles collected at S1, S2, and S3 in all haze episodes during sampling period. **(b)** Size distributions of 269, 173, and 297 type 1–3 OM particles collected at S1, S2, and S3 in one haze episode during 14–15 December.

### 3.4 Size distribution of OM-containing particles

Figure 7a shows size distributions of OM-containing particles at the three sampling sites. Aerosol particles collected at S2 and S3 display a similar peak at  $\sim 400$  nm, much smaller than the peak at 600 nm at the S1 site (Fig. 7a). This result indicates that sizes of locally emitted OM-containing particles were much larger than the long-range-transported OM-containing particles. We further obtained size distributions of type 1–3 OM particles at the three sampling sites during one haze episode. Interestingly, type 1–3 OM particles displayed similar peaks around 350 nm at all three sampling sites (Fig. 7b). This result suggests that the type 1–3 OM sources were similar in the same haze layer over the NCP.

## 4 Discussion

### 4.1 Sources of OM-containing particles

TEM adequately characterized the morphology and mixing state of OM-containing particles in wintertime L & M hazes. We found that the type 1–3 OM (Fig. 4a–c) particles were most abundant in the hazes and that most of them were internally mixed with non-OM particles (Fig. 2). This result is consistent with one previous study which found abundant amorphous spherical OM particles in the outflow of a haze plume in East Asia (Zhu et al., 2013). Moreover, Li et al. (2012) found large amounts of type 1 OM particles in a coal-burning region in China's Loess Plateau in winter. However, some studies have only found abundant type 5–6 OM particles in the atmosphere and only a few type 1–3 OM particles in urban and remote mountain air in China (Li and Shao, 2010; Li et al., 2015). Based on these comparisons, we conclude that those type 1–3 OM particles were not directly emitted by vehicular emissions in the NCP.

It should be noted that recent studies did not find abundant type 1–3 OM particles at three sampling sites in haze episodes caused by industries, coal-fired power plants and vehicular emissions in spring and summer (W. J. Li et al., 2011a; Yuan et al., 2015). However, these abundant type 1–3 OM particles occurred in haze episodes over a coal-burning haze caused by house heating, heavy industries, and residential stoves in the China Loess Plateau in winter (Li et al., 2012). Based on the comparisons, we may exclude that large amount of type 1–3 OM particles could be directly emitted from coal-fired power plants and heavy industries. Zhang et al. (2008) suggested that industrial boilers had cleaner combustion with much less by-product of particulate carbon and with much lower levels of OM, while residential stoves had significantly higher emissions of carbonaceous particulate matter with emission rates 100 times higher than that of industrial boilers. In addition, recent studies have found that uncontrolled solid fuels combustion in households had a major effect on haze episode in Beijing through aerosol modeling and satellite monitoring (Ru et al., 2015; J. Liu et al., 2016). As a result, we believe that the type 1–3 OM particles can mainly be emitted by coal combustion and biomass burning in households while not emitted from vehicular, heavy industries, or coal-fired power plants in wintertime. In particular, the abundant near-spherical OM particles with higher Sph and lower AR indicate that these OM particles formed in cooling process after polluted plumes emitted from coal combustion and biomass burning.

Biomass burning and coal combustion both can produce types 1–3 OM particles and all contain a certain amount of Si in addition to C and O (Li et al., 2012; Posfai et al., 2004; Hand et al., 2005; Adachi and Buseck, 2011). Li et al. (2012) found that primary OM particles contain much higher Si from coal combustion than biomass burning. Although EDX can only obtain semiquantitative C, O, and Si from OM par-



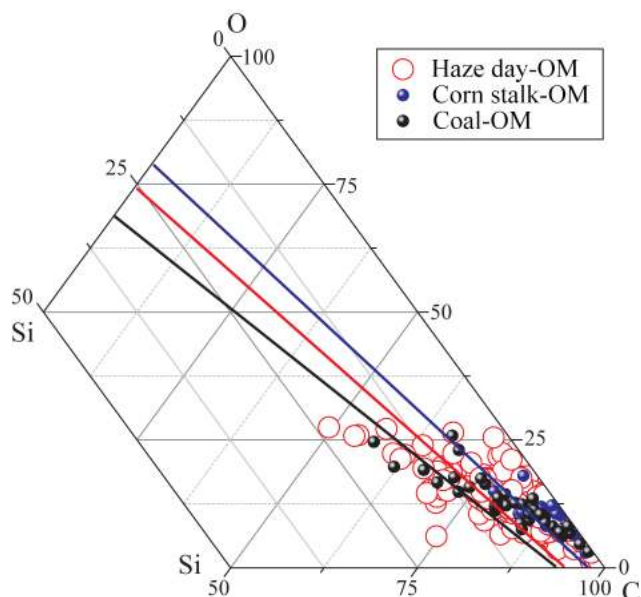


**Figure 8.** Triangular diagram of weight ratios of Si-O-C based on TEM/EDX data. A total of 39 OM particles are from coal combustion and 28 OM particles from corn stalks combustion, as well as 281 OM particles produced from the haze samples in this study. The three lines represent the connection of Si / O and Si / C for different OM particles.

ticles, the ratios of C-O-Si were comparable in different OM particles (Fig. 8). To evaluate OM sources in this study, we compared ratios of Si, O, and C in individual OM particles collected in haze (281 OM particles) and fresh OM particles from corn stalks (28 OM particles) and coal combustion (39 OM particles) conducted in the laboratory (see the Supplement). Figure 8 shows that the haze OM particles were more associated with coal combustion compared with corn stalks from the point of coverage. The haze OM line is located between corn stalks and coal combustion (Fig. 8). This result revealed that the Si ratio in individual OM particles is ordered as coal combustion > haze particles > corn stalks, and that 71 % of haze OM particles are associated with coal combustion. Based on the result, we can estimate that coal combustion contributes more type 1–3 OM particles than biomass burning in the wintertime L & M haze. This result is consistent with the source apportionment of OM particles based on their mass concentrations (Elser et al., 2016; Sun et al., 2013).

#### 4.2 Ageing of OM particles

The complicated mixing structures of individual particles can be used to evaluate particle ageing mechanisms (W. Li et al., 2016). It is well known that S2 and S3, as the polluted background sites, received aged particles after long-range transport and that the urban site, S1, received more fresh particles. Indeed, OM-soot particles at S2 and S3 sites were internally

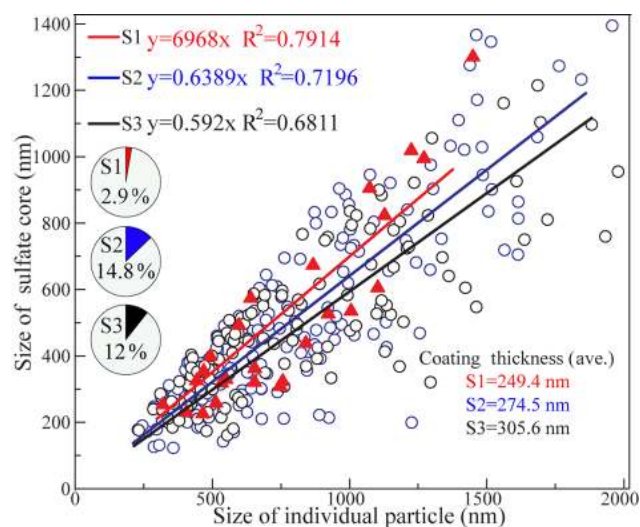


**Figure 9.** The relationship between the size of individual particles and their sulfate cores based on 366 OM-coating particles at sites S1, S2, and S3. The smaller slope represents the thicker OM coating. The number fractions of OM coating particles to OM-containing particles at three sampling sites are shown in the pie charts.

mixed with sulfates but not at S1 (Figs. 6 and S8). To evaluate particle ageing processes, we measured OM coating thickness in type 6 OM-coating particles (e.g., Fig. 5e) because coating thickness on secondary particles can be used to infer particle ageing during transport (Moffet et al., 2010, 2013). In this study, OM coating thickness increased with particle size and their average values at the three sampling sites were ordered as S3 > S2 > S1 (i.e., 249.4 nm at S1, 274.5 nm at S2, and 305.6 nm at S3) (Fig. 9). The results suggest that particles with larger sizes underwent more ageing than the fine particles and that the particles at S3 underwent the most ageing. However, number fractions of type 6 OM particles were small at three sampling sites (2.9 % at S1, 14.8 % at S2, and 12 % at S3) (Fig. 9). This phenomenon may be caused by the weak atmospheric reactions for SOA formation in the whole haze layer.

## 5 Conclusions and atmospheric implications

Abundant type 1–3 OM particles at S1, S2, and S3 suggested that coal combustion and biomass burning used for cooking and heating in the residential sector in winter significantly contributed to the haze layer over the NCP. Although heavy industrial and coal-fired plants emitted large amount of gases such as SO<sub>2</sub>, NO<sub>x</sub>, and VOCs in the NCP (X. Wang et al., 2012; M. Wang et al., 2013; Zhang et al., 2015), we did not observe an unusually large number of secondary organic and inorganic aerosols in wintertime L & M hazes; these aerosols are common particle types in heavy haze and fog episodes (W. J. Li et al., 2011b). The results indicated very

weak photochemical reactions due to lower O<sub>3</sub> concentrations and weaker solar radiation, two constraints that reduce the conversion of the acidic gases into aerosol particles (Ma et al., 2012). Also, the L & M hazes were dry with RH < 60 % (Fig. S5), which prohibits heterogeneous reactions between particles and gases (Zheng et al., 2015). These reasons can explain why we found higher number and mass fractions of abundant type 1–3 primary OM particles and lower type 6 secondary OM particles in the hazes. This result is consistent with a previous study using AMS (Sun et al., 2013), which showed 69 % primary OM particles and only 31 % SOA in winter L & M hazes.

Our microscopic observations of individual particles provide direct evidence on the regional L & M haze formation in NCP, which is mainly caused by the residential coal stoves used for heating and cooking in winter. The result is consistent with the large-scale modeling studies and the field campaign in the NCP from recent studies (P. Liu et al., 2016; J. Liu et al., 2016; Ru et al., 2015). Therefore, we can conclude that these studies prove that these residential coal stoves in rural areas and in the urban outskirts have no pollution controls and directly emit particulate carbon and other pollutants. The emission control of residential coarse coal combustion is simply not regulated by the national environmental protection bureau, even though this bureau has made much recent progress in controlling emissions from heavy industries and coal-fired power plants.

Our study indicated that measures should be taken to control the wide range of residential coal stoves in the NCP in wintertime. The type 1–3 OM particles from residential stoves mainly consist of PAHs (Zhang et al., 2008). In this study, we found that type 1–3 OM particles not only occurred in 68 % of OM-containing aerosol particles but were also concentrated on fine particles (< 1 μm) (Fig. 7a). Therefore, OM-containing particles in the frequent L & M hazes could pose a threat to human health throughout the winter. These microscopic observations results should be compared with models to evaluate our understanding of OM particles on human health and climate and to acquire their hygroscopic and optical properties in L & M haze episodes.

## 6 Data availability

All the data presented in this paper are available upon request. Please contact the corresponding author (liweijun\_atmos@gmail.com or liweijun@sdu.edu.cn).

**The Supplement related to this article is available online at doi:10.5194/acp-17-1259-2017-supplement.**

*Competing interests.* The authors declare that they have no conflict of interest.

*Acknowledgements.* We appreciate Peter Hyde's comments and proofreading. This work was funded by the National Natural Science Foundation of China (41575116 and 41622504), the National Key Project of MOST (JFY2016ZY01002213), International Cooperation and Exchange project, the National Natural Science Foundation of China (41571130033), and the Shandong Provincial Science Fund for Distinguished Young Scholars, China (JQ201413).

Edited by: T. Zhu

Reviewed by: three anonymous referees

## References

- Adachi, K. and Buseck, P. R.: Atmospheric tar balls from biomass burning in Mexico, *J. Geophys. Res.*, 116, D05204, doi:10.1029/2010jd015102, 2011.
- Alexander, D. T. L., Crozier, P. A., and Anderson, J. R.: Brown Carbon Spheres in East Asian Outflow and Their Optical Properties, *Science*, 321, 833–836, doi:10.1126/science.1155296, 2008.
- Chakrabarty, R. K., Moosmüller, H., Chen, L.-W. A., Lewis, K., Arnott, W. P., Mazzoleni, C., Dubey, M. K., Wold, C. E., Hao, W. M., and Kreidenweis, S. M.: Brown carbon in tar balls from smoldering biomass combustion, *Atmos. Chem. Phys.*, 10, 6363–6370, doi:10.5194/acp-10-6363-2010, 2010.
- Chakrabarty, R. K., Arnold, I. J., Francisco, D. M., Hatchett, B., Hosseinpour, F., Loria, M., Pokharel, A., and Woody, B. M.: Black and brown carbon fractal aggregates from combustion of two fuels widely used in Asian rituals, *J. Quant. Spectrosc. Ra.*, 122, 25–30, doi:10.1016/j.jqsrt.2012.12.011, 2013.
- Chen, J., Qiu, S., Shang, J., Wilfrid, O. M., Liu, X., Tian, H., and Boman, J.: Impact of relative humidity and water soluble constituents of PM<sub>2.5</sub> on visibility impairment in Beijing, China, *Aerosol Air Qual. Res.*, 14, 260–268, doi:10.4209/aaqr.2012.12.0360, 2014.
- Chi, J. W., Li, W. J., Zhang, D. Z., Zhang, J. C., Lin, Y. T., Shen, X. J., Sun, J. Y., Chen, J. M., Zhang, X. Y., Zhang, Y. M., and Wang, W. X.: Sea salt aerosols as a reactive surface for inorganic and organic acidic gases in the Arctic troposphere, *Atmos. Chem. Phys.*, 15, 11341–11353, doi:10.5194/acp-15-11341-2015, 2015.
- China, S., Mazzoleni, C., Gorkowski, K., Aiken, A. C., and Dubey, M. K.: Morphology and mixing state of individual freshly emitted wildfire carbonaceous particles, *Nat. Commun.*, 4, 2122, doi:10.1038/ncomms3122, 2013.
- Elser, M., Huang, R.-J., Wolf, R., Slowik, J. G., Wang, Q., Canonaco, F., Li, G., Bozzetti, C., Daellenbach, K. R., Huang, Y., Zhang, R., Li, Z., Cao, J., Baltensperger, U., El-Haddad, I., and Prévôt, A. S. H.: New insights into PM<sub>2.5</sub> chemical composition and sources in two major cities in China during extreme haze events using aerosol mass spectrometry, *Atmos. Chem. Phys.*, 16, 3207–3225, doi:10.5194/acp-16-3207-2016, 2016.
- Feng, J. L., Guo, Z. G., Zhang, T. R., Yao, X. H., Chan, C. K., and Fang, M.: Source and formation of secondary particulate matter in PM<sub>2.5</sub> in Asian continental outflow, *J. Geophys. Res.-Atmos.*, 117, D03302, doi:10.1029/2011jd016400, 2012.
- Fu, P. Q., Kawamura, K., Chen, J., Li, J., Sun, Y. L., Liu, Y., Tachibana, E., Aggarwal, S. G., Okuzawa, K., Tanimoto, H., Kanaya, Y., and Wang, Z. F.: Diurnal variations of organic molec-

- ular tracers and stable carbon isotopic composition in atmospheric aerosols over Mt. Tai in the North China Plain: an influence of biomass burning, *Atmos. Chem. Phys.*, 12, 8359–8375, doi:10.5194/acp-12-8359-2012, 2012.
- Fuzzi, S., Andreae, M. O., Huebert, B. J., Kulmala, M., Bond, T. C., Boy, M., Doherty, S. J., Guenther, A., Kanakidou, M., Kawamura, K., Kerminen, V.-M., Lohmann, U., Russell, L. M., and Pöschl, U.: Critical assessment of the current state of scientific knowledge, terminology, and research needs concerning the role of organic aerosols in the atmosphere, climate, and global change, *Atmos. Chem. Phys.*, 6, 2017–2038, doi:10.5194/acp-6-2017-2006, 2006.
- Ghosal, S., Weber, P. K., and Laskin, A.: Spatially resolved chemical imaging of individual atmospheric particles using nanoscale imaging mass spectrometry: insight into particle origin and chemistry, *Anal. Methods*, 6, 2444–2451, doi:10.1039/c3ay42012d, 2014.
- Guo, S., Hu, M., Zamora, M. L., Peng, J., Shang, D., Zheng, J., Du, Z., Wu, Z., Shao, M., Zeng, L., Molina, M. J., and Zhang, R.: Elucidating severe urban haze formation in China, *P. Natl. Acad. Sci. USA*, 111, 17373–17378, doi:10.1073/pnas.1419604111, 2014.
- Hand, J. L., Malm, W. C., Laskin, A., Day, D., Lee, T., Wang, C., Carrico, C., Carrillo, J., Cowin, J. P., Collett, J., and Iedema, M. J.: Optical, physical, and chemical properties of tar balls observed during the Yosemite Aerosol Characterization Study, *J. Geophys. Res.*, 110, D21210, doi:10.1029/2004jd005728, 2005.
- Huang, R. J., Zhang, Y., Bozzetti, C., Ho, K. F., Cao, J. J., Han, Y., Daellenbach, K. R., Slowik, J. G., Platt, S. M., Canonaco, F., Zotter, P., Wolf, R., Pieber, S. M., Bruns, E. A., Crippa, M., Ciarelli, G., Piazzalunga, A., Schwikowski, M., Abbaszade, G., Schnelle-Kreis, J., Zimmermann, R., An, Z., Szidat, S., Baltensperger, U., El Haddad, I., and Prevot, A. S.: High secondary aerosol contribution to particulate pollution during haze events in China, *Nature*, 514, 218–222, doi:10.1038/nature13774, 2014.
- Kanakidou, M., Seinfeld, J. H., Pandis, S. N., Barnes, I., Dentener, F. J., Facchini, M. C., Van Dingenen, R., Ervens, B., Nenes, A., Nielsen, C. J., Swietlicki, E., Putaud, J. P., Balkanski, Y., Fuzzi, S., Horth, J., Moortgat, G. K., Winterhalter, R., Myhre, C. E. L., Tsigaridis, K., Vignati, E., Stephanou, E. G., and Wilson, J.: Organic aerosol and global climate modelling: a review, *Atmos. Chem. Phys.*, 5, 1053–1123, doi:10.5194/acp-5-1053-2005, 2005.
- Kulmala, M., Kerminen, V.-M., Anttila, T., Laaksonen, A., and O'Dowd, C. D.: Organic aerosol formation via sulphate cluster activation, *J. Geophys. Res.-Atmos.*, 109, D04205, doi:10.1029/2003JD003961, 2004.
- Li, K., Sinha, B., and Hoppe, P.: Speciation of Nitrogen-Bearing Species Using Negative and Positive Secondary Ion Spectra with Nano Secondary Ion Mass Spectrometry, *Anal. Chem.*, 88, 3281–3288, doi:10.1021/acs.analchem.5b04740, 2016.
- Li, W., Li, P., Sun, G., Zhou, S., Yuan, Q., and Wang, W.: Cloud residues and interstitial aerosols from non-precipitating clouds over an industrial and urban area in northern China, *Atmos. Environ.*, 45, 2488–2495, doi:10.1016/j.atmosenv.2011.02.044, 2011.
- Li, W., Shi, Z., Zhang, D., Zhang, X., Li, P., Feng, Q., Yuan, Q., and Wang, W.: Haze particles over a coal-burning region in the China Loess Plateau in winter: Three flight missions in December 2010, *J. Geophys. Res.*, 117, D12306, doi:10.1029/2012jd017720, 2012.
- Li, W., Wang, T., Zhou, S., Lee, S., Huang, Y., Gao, Y., and Wang, W.: Microscopic Observation of Metal-Containing Particles from Chinese Continental Outflow Observed from a Non-Industrial Site, *Environ. Sci. Technol.*, 47, 9124–9131, doi:10.1021/es400109q, 2013.
- Li, W., Shao, L., Zhang, D., Ro, C.-U., Hu, M., Bi, X., Geng, H., Matsuki, A., Niu, H., and Chen, J.: A review of single aerosol particle studies in the atmosphere of East Asia: morphology, mixing state, source, and heterogeneous reactions, *J. Clean. Prod.*, 112, 1330–1349, doi:10.1016/j.jclepro.2015.04.050, 2016.
- Li, W. J. and Shao, L. Y.: Mixing and water-soluble characteristics of particulate organic compounds in individual urban aerosol particles, *J. Geophys. Res.*, 115, D02301, doi:10.1029/2009JD012575, 2010.
- Li, W. J., Zhang, D. Z., Shao, L. Y., Zhou, S. Z., and Wang, W. X.: Individual particle analysis of aerosols collected under haze and non-haze conditions at a high-elevation mountain site in the North China plain, *Atmos. Chem. Phys.*, 11, 11733–11744, doi:10.5194/acp-11-11733-2011, 2011a.
- Li, W. J., Zhou, S. Z., Wang, X. F., Xu, Z., Yuan, C., Yu, Y. C., Zhang, Q. Z., and Wang, W. X.: Integrated evaluation of aerosols from regional brown hazes over northern China in winter: Concentrations, sources, transformation, and mixing states, *J. Geophys. Res.*, 116, D09301, doi:10.1029/2010jd015099, 2011b.
- Li, W. J., Chen, S. R., Xu, Y. S., Guo, X. C., Sun, Y. L., Yang, X. Y., Wang, Z. F., Zhao, X. D., Chen, J. M., and Wang, W. X.: Mixing state and sources of submicron regional background aerosols in the northern Qinghai–Tibet Plateau and the influence of biomass burning, *Atmos. Chem. Phys.*, 15, 13365–13376, doi:10.5194/acp-15-13365-2015, 2015.
- Liu, J., Mauzerall, D. L., Chen, Q., Zhang, Q., Song, Y., Peng, W., Klimont, Z., Qiu, X., Zhang, S., Hu, M., Lin, W., Smith, K. R., and Zhu, T.: Air pollutant emissions from Chinese households: A major and underappreciated ambient pollution source, *P. Natl. Acad. Sci. USA*, 113, 7756–7761, doi:10.1073/pnas.1604537113, 2016.
- Liu, P., Zhang, C., Mu, Y., Liu, C., Xue, C., Ye, C., Liu, J., Zhang, Y., and Zhang, H.: The possible contribution of the periodic emissions from farmers' activities in the North China Plain to atmospheric water-soluble ions in Beijing, *Atmos. Chem. Phys.*, 16, 10097–10109, doi:10.5194/acp-16-10097-2016, 2016.
- Ma, J., Xu, X., Zhao, C., and Yan, P.: A review of atmospheric chemistry research in China: Photochemical smog, haze pollution, and gas-aerosol interactions, *Adv. Atmos. Sci.*, 29, 1006–1026, doi:10.1007/s00376-012-1188-7, 2012.
- Mauderly, J. L. and Chow, J. C.: Health Effects of Organic Aerosols, *Inhal. Toxicol.*, 20, 257–288, doi:10.1080/089583707018666008, 2008.
- Moffet, R. C., Henn, T. R., Tivanski, A. V., Hopkins, R. J., Desyaterik, Y., Kilcoyne, A. L. D., Tylliszczak, T., Fast, J., Barnard, J., Shutthanandan, V., Cliff, S. S., Perry, K. D., Laskin, A., and Gilles, M. K.: Microscopic characterization of carbonaceous aerosol particle aging in the outflow from Mexico City, *Atmos. Chem. Phys.*, 10, 961–976, doi:10.5194/acp-10-961-2010, 2010.
- Moffet, R. C., Rödel, T. C., Kelly, S. T., Yu, X. Y., Carroll, G. T., Fast, J., Zaveri, R. A., Laskin, A., and Gilles, M. K.: Spectro-microscopic measurements of carbonaceous aerosol aging in Central California, *Atmos. Chem. Phys.*, 13, 10445–10459, doi:10.5194/acp-13-10445-2013, 2013.

- Pöschl, U.: Atmospheric aerosols: composition, transformation, climate and health effects, *Angew. Chem. Int. Edit.*, 44, 7520–7540, doi:10.1002/anie.200501122, 2005.
- Posfai, M., Gelencser, A., Simonics, R., Arato, K., Li, J., Hobbs, P. V., and Buseck, P. R.: Atmospheric tar balls: Particles from biomass and biofuel burning, *J. Geophys. Res.-Atmos.*, 109, D06213, doi:10.1029/2003JD004169, 2004.
- Riipinen, I., Pierce, J. R., Yli-Juuti, T., Nieminen, T., Häkkinen, S., Ehn, M., Junninen, H., Lehtipalo, K., Petäjä, T., Slowik, J., Chang, R., Shantz, N. C., Abbatt, J., Leaitch, W. R., Kerminen, V.-M., Worsnop, D. R., Pandis, S. N., Donahue, N. M., and Kulmala, M.: Organic condensation: a vital link connecting aerosol formation to cloud condensation nuclei (CCN) concentrations, *Atmos. Chem. Phys.*, 11, 3865–3878, doi:10.5194/acp-11-3865-2011, 2011.
- Ru, M., Tao, S., Smith, K., Shen, G., Shen, H., Huang, Y., Chen, H., Chen, Y., Chen, X., Liu, J., Li, B., Wang, X., and He, C.: Direct Energy Consumption Associated Emissions by Rural-to-Urban Migrants in Beijing, *Environ. Sci. Technol.*, 49, 13708–13715, doi:10.1021/acs.est.5b03374, 2015.
- Shen, X. J., Sun, J. Y., Zhang, X. Y., Zhang, Y. M., Zhang, L., Che, H. C., Ma, Q. L., Yu, X. M., Yue, Y., and Zhang, Y. W.: Characterization of submicron aerosols and effect on visibility during a severe haze-fog episode in Yangtze River Delta, China, *Atmos. Environ.*, 120, 307–316, doi:10.1016/j.atmosenv.2015.09.011, 2015.
- Shiraiwa, M., Ammann, M., Koop, T., and Pöschl, U.: Gas uptake and chemical aging of semisolid organic aerosol particles, *P. Natl. Acad. Sci. USA*, 108, 11003–11008, doi:10.1073/pnas.1103045108, 2011.
- Sun, Y. L., Zhang, Q., Anastasio, C., and Sun, J.: Insights into secondary organic aerosol formed via aqueous-phase reactions of phenolic compounds based on high resolution mass spectrometry, *Atmos. Chem. Phys.*, 10, 4809–4822, doi:10.5194/acp-10-4809-2010, 2010.
- Sun, Y. L., Wang, Z. F., Fu, P. Q., Yang, T., Jiang, Q., Dong, H. B., Li, J., and Jia, J. J.: Aerosol composition, sources and processes during wintertime in Beijing, China, *Atmos. Chem. Phys.*, 13, 4577–4592, doi:10.5194/acp-13-4577-2013, 2013.
- Wang, G., Kawamura, K., Xie, M., Hu, S., Cao, J., An, Z., Waston, J. G., and Chow, J. C.: Organic Molecular Compositions and Size Distributions of Chinese Summer and Autumn Aerosols from Nanjing: Characteristic Haze Event Caused by Wheat Straw Burning, *Environ. Sci. Technol.*, 43, 6493–6499, doi:10.1021/es803086g, 2009.
- Wang, J., Zhang, Y., Shao, M., Liu, X., Zheng, L., Cheng, C., and Xu, X.: Quantitative relationship between visibility and mass concentration of PM<sub>2.5</sub> in Beijing, *J. Environ. Sci.*, 18, 475–481, 2006.
- Wang, M., Shao, M., Lu, S.-H., Yang, Y.-D., and Chen, W.-T.: Evidence of coal combustion contribution to ambient VOCs during winter in Beijing, *Chinese Chem. Lett.*, 24, 829–832, doi:10.1016/j.ccllet.2013.05.029, 2013.
- Wang, X., Wang, W., Yang, L., Gao, X., Nie, W., Yu, Y., Xu, P., Zhou, Y., and Wang, Z.: The secondary formation of inorganic aerosols in the droplet mode through heterogeneous aqueous reactions under haze conditions, *Atmos. Environ.*, 63, 68–76, doi:10.1016/j.atmosenv.2012.09.029, 2012.
- You, Y., Renbaum-Wolff, L., Carreras-Sospedra, M., Hanna, S. J., Hiranuma, N., Kamal, S., Smith, M. L., Zhang, X., Weber, R. J., Shilling, J. E., Dabdub, D., Martin, S. T., and Bertram, A. K.: Images reveal that atmospheric particles can undergo liquid–liquid phase separations, *P. Natl. Acad. Sci. USA*, 109, 13188–13193, doi:10.1073/pnas.1206414109, 2012.
- Yuan, Q., Li, W., Zhou, S., Yang, L., Chi, J., Sui, X., and Wang, W.: Integrated evaluation of aerosols during haze-fog episodes at one regional background site in North China Plain, *Atmos. Res.*, 156, 102–110, doi:10.1016/j.atmosres.2015.01.002, 2015.
- Zawadowicz, M. A., Proud, S. R., Seppäläinen, S. S., and Cziczó, D. J.: Hygroscopic and phase separation properties of ammonium sulfate/organics/water ternary solutions, *Atmos. Chem. Phys.*, 15, 8975–8986, doi:10.5194/acp-15-8975-2015, 2015.
- Zhang, Q., Jimenez, J. L., Canagaratna, M. R., Allan, J. D., Coe, H., Ulbrich, I., Alfarra, M. R., Takami, A., Middlebrook, A. M., Sun, Y. L., Dzepina, K., Dunlea, E., Docherty, K., DeCarlo, P. F., Salcedo, D., Onasch, T., Jayne, J. T., Miyoshi, T., Shimono, A., Hatakeyama, S., Takegawa, N., Kondo, Y., Schneider, J., Drewnick, F., Borrmann, S., Weimer, S., Demerjian, K., Williams, P., Bower, K., Bahreini, R., Cottrell, L., Griffin, R. J., Rautiainen, J., Sun, J. Y., Zhang, Y. M., and Worsnop, D. R.: Ubiquity and dominance of oxygenated species in organic aerosols in anthropogenically-influenced Northern Hemisphere midlatitudes, *Geophys. Res. Lett.*, 34, L13801, doi:10.1029/2007gl029979, 2007.
- Zhang, X. Y., Wang, J. Z., Wang, Y. Q., Liu, H. L., Sun, J. Y., and Zhang, Y. M.: Changes in chemical components of aerosol particles in different haze regions in China from 2006 to 2013 and contribution of meteorological factors, *Atmos. Chem. Phys.*, 15, 12935–12952, doi:10.5194/acp-15-12935-2015, 2015.
- Zhang, Y., Schauer, J. J., Zhang, Y., Zeng, L., Wei, Y., Liu, Y., and Shao, M.: Characteristics of particulate carbon emissions from real-world Chinese coal combustion, *Environ. Sci. Technol.*, 42, 5068–5073, doi:10.1021/es7022576, 2008.
- Zheng, G. J., Duan, F. K., Su, H., Ma, Y. L., Cheng, Y., Zheng, B., Zhang, Q., Huang, T., Kimoto, T., Chang, D., Pöschl, U., Cheng, Y. F., and He, K. B.: Exploring the severe winter haze in Beijing: the impact of synoptic weather, regional transport and heterogeneous reactions, *Atmos. Chem. Phys.*, 15, 2969–2983, doi:10.5194/acp-15-2969-2015, 2015.
- Zhu, J., Crozier, P. A., and Anderson, J. R.: Characterization of light-absorbing carbon particles at three altitudes in East Asian outflow by transmission electron microscopy, *Atmos. Chem. Phys.*, 13, 6359–6371, doi:10.5194/acp-13-6359-2013, 2013.